Bulletin of Mathematical Biology (2022) 84:8
https://doi.org/10.1007/s11538-021-00968-3

Society for Mathematical Biology

ORIGINAL ARTICLE

Modelling Cellular Interactions and Dynamics During Kidney Morphogenesis

Blake Cook[1,2] · Alex Combes[3] · Melissa Little[4,5] · James M. Osborne[1]

Received: 29 June 2021 / Accepted: 2 November 2021 / Published online: 27 November 2021

Abstract

Kidney disease and renal disorders account for a significant proportion of health complications in mid-late adulthood worldwide. Many renal deficiencies are due to improper formation of the kidneys before birth, which are caused by disorders in the developmental process that arise from genetic and/or environmental factors. Mathematical modelling can help build on experimental knowledge to increase our understanding of the complexities of kidney organogenesis. In this paper, we present a discrete cell-based model of kidney development. Specifically, we model the tip of the developing ureteric tree to investigate the behaviours of cap mesenchyme cells which are required to sustain ureteric tip growth. We find that spatial regulation of the differentiation of cap mesenchyme cells through cellular signalling is sufficient to ensure robust ureteric tip development. Additionally, we find that increased adhesion interactions between cap mesenchyme cells and the ureteric tip surface can lead to a more stable tip-cap unit. Our analysis of the various processes on this scale highlights essential components for healthy kidney growth and provides insight into mechanisms to be studied further in order to replicate the process *in vitro*.

✉ James M. Osborne
jmosborne@unimelb.edu.au

Blake Cook
bjc926@student.bham.ac.uk

Alex Combes
alex.combes@monash.edu

Melissa Little
melissa.little@mcri.edu.au

1 School of Mathematics and Statistics, University of Melbourne, Victoria 3010, Australia

2 Present Address: Institute of Metabolism and Systems Research, College of Medical and Dental Science, University of Birmingham, Edgbaston, Birmingham B15 2TT, UK

3 Department of Anatomy and Developmental Biology, and Stem Cells and Development Program, Monash Biomedicine Discovery Institute, Monash University, Clayton, VIC 3800, Australia

4 Murdoch Children's Research Institute, Flemington Rd, Parkville, VIC 3052, Australia

5 Department of Pediatrics, University of Melbourne, Melbourne, VIC 3010, Australia

Keywords Kidney development · Mathematical biology · Cell-based modelling · Cap mesenchyme · Chaste

1 Introduction

Kidney disease and renal dysfunction are major health concerns worldwide, which as of 2017 impact the lives of 9.8% of the global population (Cockwell and Fisher 2020). Symptoms are not usually prevalent until advanced disease progression, and many of these conditions can arise from developmental and genetic complications during kidney formation before birth (Jha et al. 2013). Nephrons are the filtration units of the kidney and play a critical role in healthy kidney function. Individuals with less nephrons tend to be at higher risk of kidney disease, which accompanies a higher risk of vascular and cardiac diseases (Jha et al. 2013; Foley et al. 1998). Treatments for chronic kidney disease impose significant costs on individuals and healthcare systems worldwide, disproportionately affecting those in developing countries (Keith et al. 2004).

It has been suggested that many kidney pathologies are genetic in origin and arise due to complications of the formation of the kidney before birth (Zandi-Nejad et al. 2006; Hildebrandt 2010). Therefore, knowledge of kidney development is integral to understanding the origins of kidney disease and may offer new avenues to prevent or treat kidney disease. Many research groups have successfully shown that miniature kidney 'organoids' can be generated from a culture of induced pluripotent stem cells (Mae et al. 2013; Takasato et al. 2015; Taguchi et al. 2014; Lam et al. 2014; Little and Combes 2019), which demonstrates it may be possible one day to grow replacement kidneys from a sample of a patient's cells. However, stem cell models of the kidney are currently unable to recapitulate the reciprocal interactions and higher order patterning that build the size and functional capacity of the kidney during embryonic development. A greater understanding of the mechanisms that maintain progenitor cell populations and branching morphogenesis may enable greater control over these processes *in vitro*. When undertaken in tandem with novel experimental developments, mathematical modelling has the opportunity to play an essential part in advancing this field.

1.1 Kidney Development

Developed kidneys are derived from two major tissues: the Ureteric Bud, and the Metanephric Mesenchyme (Dressler 2006). These tissues begin to interact when the ureteric bud grows into the metanephric mesenchyme at around 10 days of embryonic development in mouse and around 5 weeks of gestation in humans (Little and Combes 2019). Reciprocal paracrine signalling and physical cellular interactions result in the induction of ureteric tip (UT) domains at the leading edge of the ureteric bud, which is rapidly surrounded by nephron progenitor cells that form cap mesenchyme (CM) domains at the end of each tip (Combes et al. 2015). Signals produced by CM cells stimulate branching morphogenesis and maintain progenitor state in the UT and reciprocal signals from the UT promote survival and maintain CM progenitor state. A

distinct set of UT signals are produced at the tip-stalk junction and trigger nearby CM cells to differentiate into early epithelial nephron structures, which attach to the UT and gradually mature into a functioning nephron. These interactions maintain a cycle of branching and nephron induction that builds the arborised structure of the ureteric tree and the complement of nephrons required to facilitate kidney function throughout life (See Fig. 1a).

UT cells form the epithelial network of ducts in the developing kidney (Riccio et al. 2016), whereas CM cells give rise to the nephrons (Kobayashi et al. 2008; Boyle et al. 2008; Combes et al. 2015) as illustrated in Fig. 1b. CM cells guide the growth of ureteric tips and respond to regionalised signals produced by the tips to differentiate into 'primed' CM cells, which are committed to forming a nephron. Primed CM cells migrate out of the tip-cap domain and form polarised epithelial spheres called Renal Vesicles (RV), which proliferate more rapidly than CM cells (Combes et al. 2015) and represent an early nephron stage.

CM cells aggregate at the tips of newly formed ureteric branches. CM cell proliferation also varies along this axis with uncommitted CM cells in the top of the niche proliferating slower than CM cells in the bottom of the niche (Short et al. 2014). Multiple UT produced signals have been shown to support CM progenitor state including BMP, FGF, and Wnt ligands (Combes et al. 2015).

Analysis of migration tracks for over 800 CM cells suggests that CM cells are subject to paracrine signals from the UT that promote CM cell attraction and are partially maintained in place at the tip by CM-UT cell adhesion. A repulsive effect was also observed when CM cells were within one cell diameter of the tip, which may be a barrier effect produced by CM cells rebounding from the impermeable tip epithelium (Combes et al. 2016). The importance of CM–UT interactions in kidney development and disease is illustrated by loss of cell adhesion molecules, such as *Itga8* and *Kif26b* (Müller et al. 1997; Uchiyama et al. 2010) that result in failure of ureteric bud outgrowth or impaired branching. Similarly, recent work has shown that impaired branching and reduced nephron number phenotypes associated with knockout of the *Wnt11* gene are due to a loss of stable cellular interactions between CM and UT cells (O'Brien et al. 2018).

Genetic or environmental disruptions affecting interactions between these critical cell populations can cause congenital abnormalities, such as absent, malformed, or small kidneys, leading to infant mortality or increased susceptibility to renal disease later in life (Short and Smyth 2016). Despite an emerging understanding of key signals and cellular dynamics in this system it is still unclear whether, and how molecular gradients across the tip affect CM differentiation. Similarly, the importance of cellular interactions in sustaining tip-cap structure is poorly understood. To address these issues, we utilise methods from computational biology to construct a simplified model of the tip-cap unit and investigate the necessary dynamics to sustain emergent tissue growth.

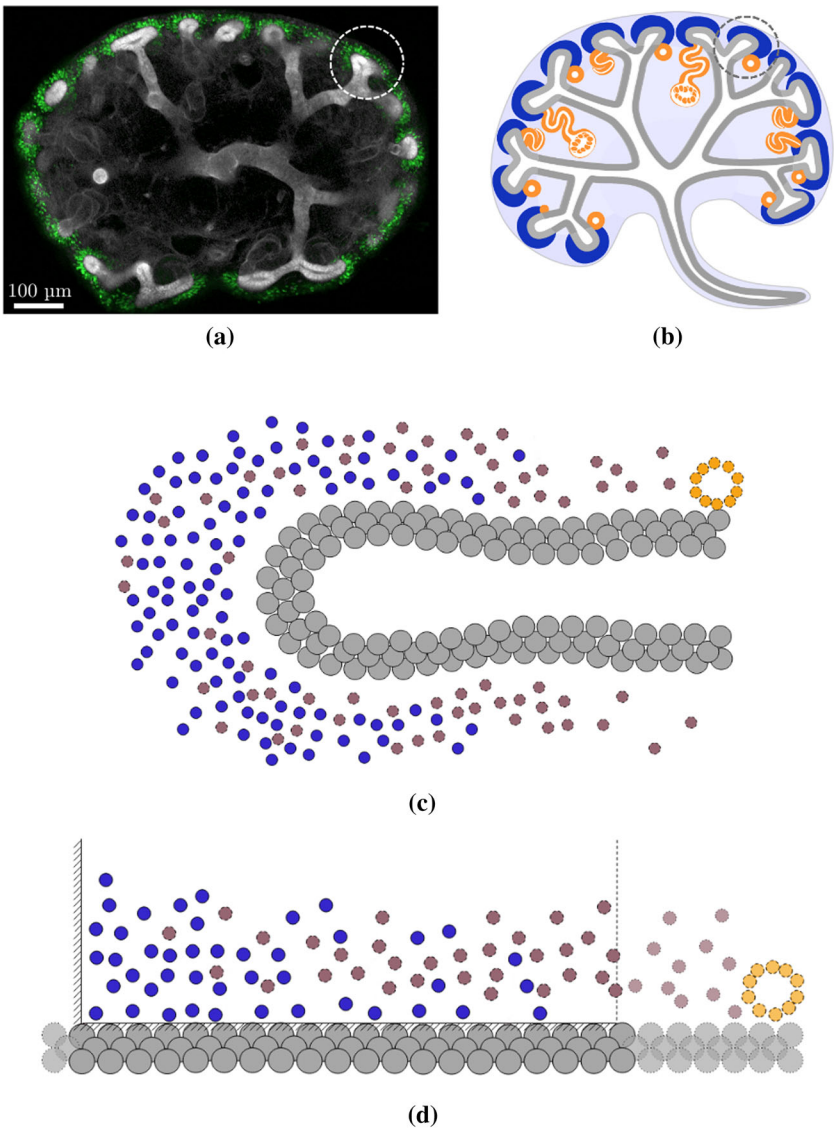

Fig. 1 Diagrams of the biological system and simulation geometry. **a** Image of developing mouse kidney and recurring UT-CM units at embryonic day (E) 14.5. Immunofluorescence for SIX2 (green) labels cap mesenchyme (CM) cells, CALB1 (white) labels the ureteric epithelium and outlines developing nephrons. Growth of kidneys occurs through a branching process, which sprouts from a tip progenitor pool and progressively forms the ureteric tree. This recurring structure (within circled region) is our target for modelling in order to understand the cellular interactions required to form a stable and consistent ureteric tip-cap unit. **b** Diagram of developing mouse kidney (Based on illustrations from Short et al. (2014)). c Two-dimensional abstraction of tip-cap unit. UT cells are shown in grey, proliferative CM cells in blue, primed CM cells in brown (not shown in b), and RV cells in orange. **d** Further abstraction of tip-cap unit to rectangular simulation domain. The bottom boundary of the simulation geometry represents the UT cells on the surface of the ureteric tip and the left simulation boundary represents 'top' of the CM, where unprimed CM cells are maintained. The right boundary represents the 'bottom' region of the tip where CM cells transition to a committed RV state (Color figure online)

1.2 Modelling Ureteric Development

Existing mathematical models for kidney development have primarily focussed on branching morphogenesis in the ureteric tree. While these models focus one level above the structures we focus on, a more global picture of the developing kidney can provide valuable insights on the characteristic time scales, signalling processes, and feedback mechanisms responsible for generating this essential organ.

Several mathematical models have been proposed and analysed for kidney development. An ordinary differential equation model proposed for kidney development was published by Zubkov et al. (2015), which described the changes and interactions of CM and UT cell populations across a spatially averaged tip-cap unit. This model incorporates a simplified description of branching and focuses on cell population numbers at a single representative tip across multiple rounds of branching. The proposed framework allows generation and investigation of hypotheses by changing physiologically representative parameters such as relative growth rates for each population, and provides insights on the outcome of number of branches in the developed kidney. Despite many simplifications and abstractions, this model was successful in replicating data from laboratory studies, as well as making new predictions. Another model of branching morphogenesis has been pursued by Hannezo et al. (2017), who developed a computational method to describe this process and replicate trends observed in number of ureteric branches and ureteric tree shape. Additionally, a multicellular model of ureteric branching was proposed by Lambert et al. (2018), which also allowed Bayesian inference of model parameters from imaging data and suggested that early branching may depend on a spatially dependent switch for cell division.

In 2013, Menshykau and Iber built on their previous work in lung morphogenesis and propose a similar Schnakenberg-type Turing mechanism model for kidney branching patterns. This partial differential equation model reproduces the observed bifurcation and trifurcation branching patterns observed in ureteric tips. Furthermore, they propose that ligand-receptor-based Turing patterns represent a general mechanism to control branching morphogenesis and other developmental processes. These methods have continued to be developed throughout publications by Okuda et al. (2018) and Menshykau et al. (2019).

However, the study of specific interactions between cells may require analysis on a smaller scale, where random fluctuations can have greater influence. Discrete cell-based modelling techniques based on methods of statistical mechanics can more accurately capture cellular interactions at this level. To this end, an investigation by Lefevre et al. in 2017 presented a discrete stochastic cell-based model on the adhesive properties of UT cells. Coupled with laboratory studies and analysis, this model was also successful in making predictions on this length scale, indicating cell-based models are an effective method for further studies of cellular interactions at the ureteric tip. Another investigation by Lawlor et al. (2019) utilised stochastic cell-based modelling to explore an experimental observation of the plasticity in CM cell priming states. Primed CM cells express the *Wnt4* gene as they progress to an RV. Previous work had shown that CM commitment to an RV state was unidirectional. Lawlor found that while this was true for the majority of the CM population, a small subset of

primed cells revert to a self-renewing unprimed state. Lineage tracing, live imaging, and single cell RNA sequencing were used to demonstrate that CM cell fate is plastic and influenced by cell migration, which mediates exposure to regionalised inductive cues. Mathematical modelling was used to explore the factors regulating CM plasticity and its effect on population stability over time. In agreement with experimental results, the majority of primed CM cells transitioned to a nephron fate. For further details, we direct the reader to the recent reviews by Short and Smyth (2017) and Short and Smyth (2020). Most mathematical models in this field focus on the branching and development of the whole kidney, rather than the stability and sustained growth of the constituent branches. In this paper, we build on computational cell-based modelling techniques and focus on the stability of the recurring ureteric tip structure.

The remainder of this paper is structured as follows: in Sect. 2, we present our stochastic computational cell-based model of cap mesenchyme cells, where we will dissect and discuss each component and how they fit together to produce a simplified model of a major cell population surrounding the ureteric tip. In Sect. 3, we present results from investigations of spatial dependence on CM cell differentiation and cap mesenchyme cell adhesion. Specifically, the questions we seek to answer are as follows: 'is cap mesenchyme growth regulated by spatially dependent factors?'; and 'how do interactions between the cap mesenchyme and the ureteric tip surface influence the commitment of the cap mesenchyme?' Finally, in Sect. 4, we discuss the biological implications on our results and discuss potential future directions for this research.

2 Multicellular Model of the Ureteric Tip

Here, we present our model for examining the factors behind robust maintenance of the cap mesenchyme progenitor population at the ureteric tip. We use a multicellular model of *unprimed/proliferative CM cells* and *primed/non-proliferative CM cells* and their interactions with the ureteric tip. We investigate the influence of proliferation, cell movement, and population growth, which underpins branching and nephron formation in the developing kidney. Our model is illustrated in Fig. 2 and the parameter descriptions and values are summarised in Table 1. Unprimed CM cells (from now on referred to as proliferative cells) are responsible for introducing new CM cells and sustaining this population, whereas primed CM cells (from now on referred to as primed cells) eventually migrate out of the modelled tip region, where they form nephrons. The lower boundary represents UT cells, which are regarded as fixed with respect to the reference frame of the model and are represented with boundary conditions on the motion of CM cells.

Throughout this section, the geometric simplification of the three-dimensional ureteric tip to the two-dimensional rectangular domain is detailed. Following this, we elaborate on the cell cycle, differentiation, and interactions implemented on the constituents of our multicellular model. We then give a brief overview of the Chaste simulation framework utilised for this investigation.

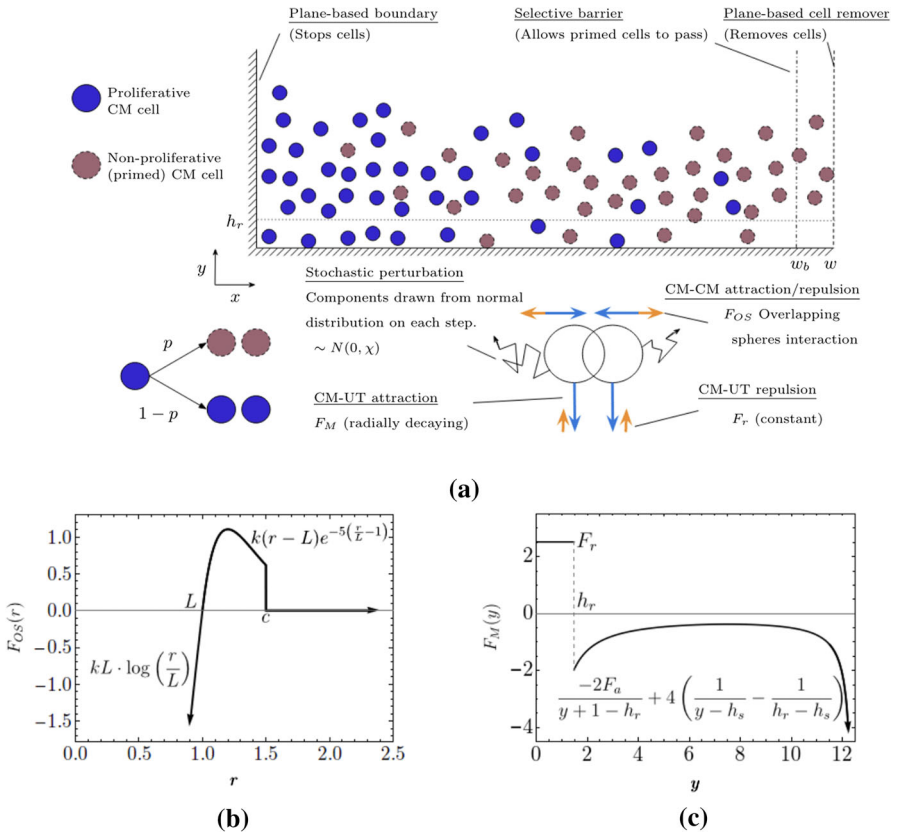

Fig. 2 Details of simulation mechanics. **a** Details on simulation boundaries, proliferation, and cell interactions. Rectangular region represents a ray of a ureteric tip where the left boundary corresponds to the top of the tip and the bottom boundary represents UT cells on the ureteric tip surface. Right boundary represents the bottom of the tip and allows only primed cells to pass and exit the simulation. The specific mechanism that maintains unprimed CM cells at the tip is not well understood, we represent this as a hard boundary in this simplified ureteric tip model. Proliferative CM cell division times are normally distributed with mean 10 h and standard deviation 2 h, division events are delayed one each time step if overcrowded. On successful division, proliferative CM cells differentiate to primed cells with probability p before dividing into two daughter cells. Cellular interactions include **b** overlapping spheres (OS) interaction force that causes attraction from a distance and repulsion when overlapping occurs. **c** CM–UT interaction forces, which includes constant short-range repulsion and long-range decaying attraction. Stochastic noise is added by implementing a cell diffusion force (Color figure online)

2.1 Simulation Geometry

In order to maintain tractability, we use a static, linear ureteric tip domain to reduce the 3D region to a simple two-dimensional rectangular region (shown in Fig. 1d).

Assuming the tip is fixed in length allows us to focus on the cellular dynamics required to sustain such a structure. We can view the fixed ureteric branch as a cylinder with a hemisphere on the top. As detailed above, regionalised factors produced by the top and bottom of the tip effectively represent a linear progression from the progenitor-

Table 1 Summary of model parameters and their default values

Parameter	Value	Units	Description	Source
Constant model parameters				
c_d	1.0	cd	Diameter of CM cells (1 cd=7.5 μm)	Combes et al. (2016)
w	20	cd	Width of simulation domain	Combes et al. (2016)
h	20	cd	Height of simulation domain	Combes et al. (2016)
w_b	18	cd	x-ordinate of semi-permeable barrier	Combes et al. (2016)
h_r	1.5	cd	Vertical distance cutoff for CM-UT repulsion force	*
h_s	12.5	cd	Height of stroma	Combes et al. (2016)
μ	10	h	Mean of division times	Short et al. (2014)
σ	2	h	Standard deviation of division times	Short et al. (2014)
V_{crit}	0.58	cd^3	Critical division volume	*
χ	0.3	kg cd h^{-2}	CM diffusion coefficient	Osborne et al. (2017)
F_a	1.0	kg cd h^{-2}	Strength of constant CM-UT attraction force	*
F_r	2.5	$\text{kg cd}^2\,\text{h}^{-2}$	Strength of linear CM-UT repulsion force	*
k	15	kg h^{-2}	CM-CM force spring constant	Mirams et al. (2013)
L	1	cd	CM-CM spring rest length	Mirams et al. (2013)
c	1.5	cd	CM-CM force cutoff length	Mirams et al. (2013)
η	1.0	kg h^{-1}	CM cell viscous drag coefficient	Mirams et al. (2013)
Varied model parameters				
p	[0,1]	non-dim	Probability of differentiation during cell division event	*
p_a	[0,1]	non-dim	Probability of primed CM cell attachment to UT	*
p_d	[0,1]	non-dim	Probability of primed CM cell detachment to UT	*
Numerical parameters				
Δt	0.005	h	Timestep	Osborne et al. (2017)

Parameters marked with an asterisk (*) were chosen here to maintain stable global behaviour. Note that the units of length in the equations used by Chaste have all been scaled by the length of a cell diameter 1 cd). One cell diameter in this simulation represents 7.5 μm (estimated from measurement data at E 12.5 from Short et al. (2014)). Specific parameters perturbed throughout this publication and numerical parameters are highlighted at the end of table

sustaining tip to the differentiation-inducing tip-stalk junction at the base. Hence, we simplify the system to two spatial dimensions by mapping the curved geometry to a rectangular domain, with the left boundary $x = 0$ corresponding to the top of the tip and the right boundary $x = w$ corresponding to the base of the tip. A sketch of this transformation is given in Fig. 1c, d. Our simulation domain is therefore a fixed rectangular region with width 20 cd (cell diameters, where 1 cell diameter is equal to 7.5 μm). The measurements for cell and ureteric bud size are based on measurement data obtained on the tip-cap structures in embryonic mouse kidneys from (Combes et al. 2016) at E 13.25 and from (Short et al. 2014) after 7-8 generations of branching. A maximum height is implemented at $y = 20$ cd, which is far outside the realistic region for CM cells. If a cell in the simulation exceeds this height then the parameter set is marked as physically unrepresentative of experimental observations.

UT cells are represented on the bottom surface of the tip domain as an impassable boundary condition at $y = 0$. That is, we assume that UT cells are rigid and fixed in position, and form an impermeable barrier. Another hard boundary condition is set on the left of the domain at $x = 0$, representing the top of the ureteric tip to keep the cells within the domain. The mechanism responsible for maintaining unprimed CM cells in this region is not well understood and requires further investigation. Here, we implement this as a hard boundary instead of something else, like a force, in order to maintain simplicity in the model so that we may focus on the interactions and transition between primed and unprimed cells responsible for stable cap formation. On the right, there is a semi-permeable boundary at $x = w_b$ that only allows primed cells to pass and exit the simulation. This represents the base of the tip, where primed CM cells (defined in next section) exit the tip-cap unit and form renal vesicles and eventually become nephrons. The midpoint $x = w_b/2$ roughly corresponds to the centre of the tip. The simulation geometry and boundary conditions are summarised in Fig. 2a.

2.2 Modelling Cap Mesenchyme Cells

Two motile sub-populations of cells are explicitly represented in our model: proliferative CM cells (shown in blue) and primed CM cells (shown in brown). Primed CM cells are committed to becoming renal vesicle (RV) cells, but this occurs outside of the simulation domain and thus not explicitly modelled. The proliferative CM cells are each given a cell cycle, which instructs the cells to divide at random times drawn from a truncated Normal distribution with mean 10 hours and standard deviation of 2 hours (and minimum 0), matching estimates of cell cycle length at E 13.25 in previous studies (Short et al. 2014). In addition to this, division events can be delayed if there is too much competition for space and resources; hence division can only occur if the effective volume of the CM cell is above a critical threshold V_{crit}, corresponding to little or no overcrowding of CM cells. Although cell death is possible via overcrowding in reality, we have omitted all cell death in this simulation, and the only removal of cells occurs when primed CM cells cross the semi-permeable right boundary.

On each successful division of proliferative cells, the resulting cells both differentiate to non-proliferative primed cells with probability p. It is likely that this probability is dependent on the cell position and time due to intracellular signalling regulating

this process, but we will omit time dependence for now and further investigate spatial dependence in the following sections. Furthermore, we assume that only symmetric division occurs, so that the two resulting cells upon division are either both proliferative or both primed (results are similar for asymmetric division at similar rates).

2.3 Forces and Cellular Interactions

Interacting cells are represented by their centres whose motion is modelled by considering their interactions through forces. Motile CM cells are subject to: attraction and repulsion forces to the bottom boundary, representing UT cells; repulsion from the stroma; and attraction and repulsion between neighbouring CM cells. We also add stochastic noise by applying a normally distributed perturbation to each cell every timestep. These forces are summarised in Fig. 2a.

Between all CM cells, attraction and repulsion are governed by an overlapping spheres interaction force (Osborne et al. 2017; Atwell et al. 2015) given by,

$$F_{OS}(r) = \begin{cases} kL \cdot \log\left(\frac{r}{L}\right), & 0 < r < L, \\ k(r-L) \cdot e^{-5\left(\frac{r}{L}-1\right)}, & L \leq r < c, \\ 0, & r \geq c, \end{cases} \tag{1}$$

where r is the distance to neighbouring cell centres, and the parameters k, L, and c are the spring constant, resting distance and cut-off distance, respectively, taken to be 4 cd in this case. This results in cells attracting together across small distances, but strong repulsion when overlapping occurs. [1] A plot of this force is given in Fig. 2b.

In order to consider the attraction and repulsion of CM cells from the UT cells we break the force up into: short-range repulsion due to physical exclusion; short- to medium-range attraction; short-range repulsion from surrounding stroma. For simplicity we assume that repulsion acting on CM cells from the UT cells is a constant force of strength F_r that acts when the CM cells are within a distance of h_r. Attraction between CM cells and UT cells appears to decay as distance increases, but then repulsion between the CM cells and the surrounding stroma pushes cells back towards UT cells. To take into account the decaying force intensity as moving away from the UT cells, and to separate the effects of the collinear force components, we define the attraction/repulsion force acting on CM cells from UT cells and the surrounding stroma as

$$F_M(y) = \begin{cases} F_r, & 0 \leq y \leq h_r, \\ \frac{-2F_a}{y+c_d-h_r} + 4\left(\frac{1}{y-h_s} - \frac{1}{h_r-h_s}\right), & h_r < y < h_s, \\ 0, & y \geq h_s. \end{cases} \tag{2}$$

where y denotes the distance of a CM cell from the UT cells, F_a and F_r are constants for the strength of UT attraction and repulsion, c_d is the typical diameter of a cell,

[1] This commonly used cellular interaction force gives a similar behaviour to a Lennard Jones type potential (used commonly in molecular dynamics). Moreover, it doesn't exhibit unstable behaviour (cluster formation) when using a linear interaction force (Pathmanathan et al. 2009).

and h_r and h_s denote the height of the effective range of UT and stroma repulsion, respectively. We set $F_M(y) = 0$ when $y > h_s$ since cells do not cross the height $y = h_s$ with this force implemented. A plot of this force is given in Fig. 2c. Attraction between CM and UT cells causes a flattening of the population across the simulation domain, thereby increasing the exit rate of CM cells in a similar fashion as increasing cell diffusion and proliferation rates. By individually isolating these factors, we have observed that the impact on exit rate is minimal compared to the effect of proliferation and diffusion of CM cells. Stochastic noise is implemented by applying a random perturbation to each cell, where each component is independently sampled from a normal distribution with zero mean and variance equal to χ.

CM cells move within an extracellular matrix with low Reynolds number; hence we may assume that the inertial components of motion are an order of magnitude smaller than the dissipative components (Purcell 1977). The equation of motion governing each cell in the simulation is thus given as, (Osborne et al. 2017),

$$\eta \frac{\mathrm{d}\mathbf{r}_i}{\mathrm{d}t} = \sum_{j \in \mathcal{N}_i(t)} \mathbf{F}_{ij}(t) + \mathbf{B}_i(t), \tag{3}$$

where η is a viscous drag coefficient, $\mathbf{F}_{ij}$ denotes the force on cell i from cell j (given by F_{OS}) and $\mathbf{B}_i(t)$ is the sum of any other forces on cell i at time t (such as chemotaxis or diffusion). We can numerically solve these ordinary differential equations (ODEs) using a forward Euler scheme

$$\mathbf{r}_i(t + \Delta t) = \mathbf{r}_i(t) + \frac{\Delta t}{\eta} \left(\sum_{j \in \mathcal{N}_i(t)} \mathbf{F}_{ij}(t) + \mathbf{B}_i(t) \right), \tag{4}$$

where Δt is the timestep. We choose Δt sufficiently small enough so that if we reduce the timestep further then simulation results are visually indistinguishable.

2.4 Simulation Framework

Our model is implemented within the open-source software suite Chaste (Cancer, Heart and Soft Tissue Environment, http://www.cs.ox.ac.uk/chaste/), which was developed for multicellular simulation and multilevel biological tissue modelling (Mirams et al. 2013; Osborne et al. 2017; Cooper et al. 2020). Chaste allows users to define their own simulation components and additionally supplies several common libraries for defining and implementing cell-cycle models, cell death events, overlapping spheres interaction forces, boundary conditions and ODE solvers. Here we have used the core mechanical libraries from chaste for cell–cell interactions and added code to represent CM–UT interactions, cell proliferation and differentiation. Additional code written for this project, along with instructions for its use, can be found at https://github.com/BlakeJC94/kidney-dev.

Simulations were run for long enough to ensure the onset of steady state in the total number of cells. Under most circumstances, we simulated for between 600 and

1000 hours with a default timestep of $\Delta t = 0.005$ and we ran 20 simulations per parameter value. All simulations were run a single core of an Intel$^{(R)}$ Xeon$^{(R)}$ E5-2683 v4 processor running at 2.10GHz (3.00GHz turbo) and 256Gb of memory. One simulation of 1000 hours with the default configuration takes about 15 minutes to complete.

3 Results

The default configuration of this model produces consistent results across multiple realisations (subject to stochastic variations). A typical simulation is shown in Fig. 3. An initial batch of proliferative CM cells diffuse and proliferate, steadily increasing the proliferative and primed sub-populations on each division. Primed CM cells passively diffuse in the positive x direction towards the selective barrier at $x = w_b$, where they are then removed from the system. Snapshots provided in Fig. 3 show minuscule changes in the system between 250 hours and 500 hours, indicating the onset of a dynamical steady state. This occurs as the exit rate of primed cells approaches the entry rate of new cells via proliferation. A stable population then settles into a spatial distribution that resembles an elliptical quadrant with semi-major axis aligned with the x-axis. We note that all simulations presented in this paper with appropriate parameters follow this form. Atypical simulations occur for extreme parameters where cells either proliferate without bound or all cells die out.

For a given configuration of parameters, we run a series of 20 simulations (unless otherwise stated), each with a different random seed.[2] For each simulation we output cell positions, velocities, proliferative states, ages, and locations and times of cell divisions, allowing full analysis of the system dynamics. Examining the evolution of the population statistics in Fig. 3e, f reveals the onset of a dynamic equilibrium, where population level statistics remain relatively constant, at around 250 hours.

Formally we must define the notion of dynamic equilibrium across a number of simulations with the same parameter configuration. Across n simulations, we will average the time series of the total population in a simulation. We define the onset of this steady state t_s as the time when the average total time series does not change from 10% of its value at t_{end}. We define a simulation to be in dynamic equilibrium if this time to steady state is greater than a suitably large threshold which here we choose to be 240 hours.

A key aspect we wish to examine is how the height of the population during dynamic equilibrium is influenced by model parameters. We will measure this by averaging the vertical position of the 10th highest[3] cell over all sample points in all simulations in steady state. Once at the dynamic equilibrium, we will sample data from 20 sample points each time series, separated by 12 hours to avoid correlation between samples.

[2] These seeds are predetermined and give rise to the same sequence of random numbers in a simulation regardless of which computer is used, ensuring our results can be replicated.

[3] To exclude statistical outliers.

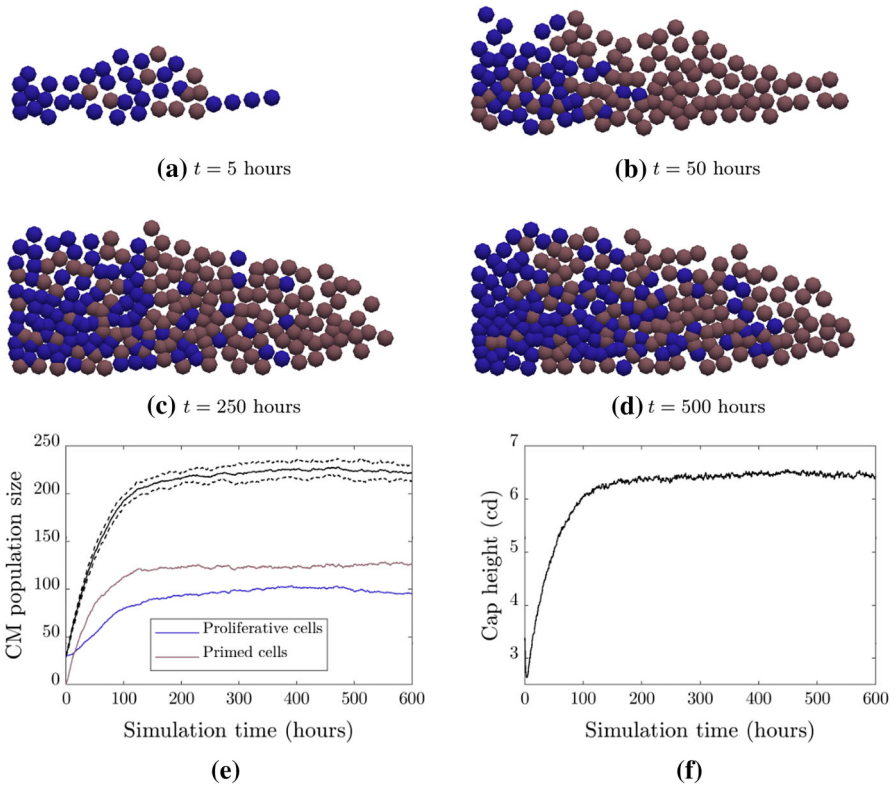

Fig. 3 Snapshots of a typical simulation with default parameters and spatial dependent differentiation at **a** 5 h, **b** 50 h, **c** 250 h, and **d** 500 h. Proliferative CM cells are shown in blue and primed CM cells are shown in brown. Also pictured are **e** average number of cells, and **f** average cap height (Color figure online)

3.1 Necessity of Spatial Dependence in CM Differentiation

The simplest model of CM cell differentiation is spatially uniform configuration, where proliferative cells differentiate to primed CM cells with probability $p = 0.5$ at all points in the domain. Intuitively, this should give a balance between proliferation and death and lead to a dynamic equilibrium. However, upon inspection of 20 simulations in Fig. 4a, we find that, while the mean population size indeed approaches a limiting value, the variation increases as some simulations result in divergence, whereas others converge to zero.

This variation across simulations can be explained by a comparison with a canonical Galton–Watson branching process, a canonical model in Probability (Watson and Galton 1875). The main result from this model (using Theorem 18.1.1 from Athreya and Lahiri 2006) tells us that for any constant $p < 1$, the proliferative population goes extinct in finite time with nonzero probability.

Such a configuration for ureteric tip development is unrealistic, since cap mesenchyme cell populations are not observed to perish in early development stages (Short et al. 2014) and instead exhibit regular sustainable tip growth and population

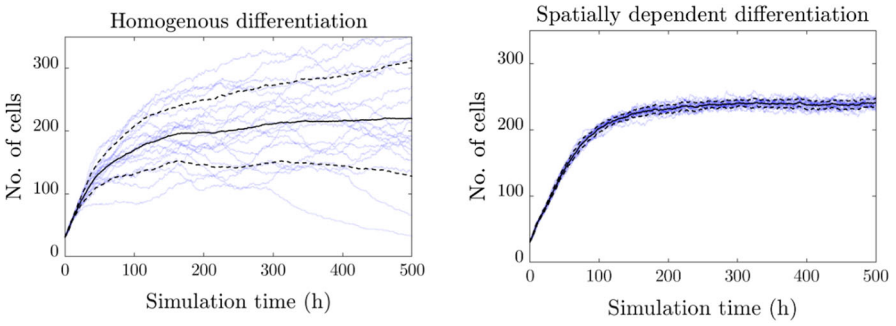

Fig. 4 Time series of the total number of cells over time across 20 different simulations under different spatial differentiation control. Twenty individual simulation outcomes (blue) are shown alongside with the mean (solid black) and standard deviation (dashed black) time series for two configurations. **a** Population size where proliferative CM cells are uniformly likely to differentiate to primed CM cells across the spatial domain. Simulations under this rule have highly variable long-term outcomes, where some instances diverge, whereas others perish. **b** Population size using a simple spatially dependent differentiation rate showing a consistent population size (Color figure online)

maintenance. In addition, the distribution of proliferative CM cells is observed to be more concentrated towards the centre/top of the tip, whereas primed cells appear to more prevalent at the base of ureteric tips where they form nephrons (Dressler 2006). This suggests the presence of a signal which is released from the top of the niche, which only allows cells to remain in a proliferative progenitor state if above a certain concentration threshold.

A simple model that reflects this signalling is to restrict differentiation based on the distance from the niche top. An example of this, where the differentiation probability p is given by $p(x) = 0$ for $0 < x < 5$ and $p(x) = 1$ for $5 < x < 20$, is shown in Fig. 4b. Specifically, we show results from 20 simulations with this non-constant proliferative rate and see that the results demonstrate a higher resemblance to the real-world behaviour of the cell population.

This comparison of results indicates that spatial regulation of CM cell progression may be responsible for the regular stable population dynamics observed in early ureteric tip development, which is supported by results from Short et al. (2014). In turn, restricted CM cell progression can also have a similar effect on tip-cap stability as increasing cell motility and decreasing the total number of cells. Restricting CM cell proliferation reduces the number of new CM cell introduced into the system, leading to fewer obstacles for the existing CM cells and thus increasing the apparent motility, giving another plausible biological explanation for these results. Hence, it can be concluded that there is a balance between increasing the CM cell proliferation/entry rate and reducing the effective diffusion that leads to a higher likelihood of a successful tip-cap unit without causing divergence of population numbers. Furthermore, the population size and composition can be changed using other parameters in Table 1, effectively establishing this as a general simplified model of niche formation at any stage in ureteric tree formation. A progressive variation in these parameters as the ureteric tree develops can explain the changes in niche size and composition through-

out the kidney development process. While a constant rate of differentiation is the simplest configuration possible, it lacks the nuance required to sustain consistent CM population dynamics, thus being insufficient to accurately model kidney development.

3.2 Dynamic Equilibrium can be Achieved Using Many Non-decreasing Differentiation Rates

We have demonstrated that some form of spatial dependence of CM cell proliferative states is a sufficient condition for sustaining a consistent tip-cap population, but what degree of spatial control is required? Specifically, what variations in dynamic steady state arise in these populations as the functional form of the probability of differentiation $p(x)$ changes? Is there a form of $p(x)$ that is more representative of the biology that can more accurately model this process?

Spatio-temporal dependence in cell division often arises through various modes of cellular communication using signalling molecules. These signals are interpreted by cells by measuring the proportion of occupied signal receptors on the cellular membrane. Models of response to these signals include: a threshold-based switch, which only requires the surrounding concentration to be above a certain level for a change in behaviour (as in the previous section); a linearly dependent response proportional to the surrounding concentration of signal; or a combination of the two.

We can implement these models of response by choosing different forms of $p(x)$,

$$p_{\text{Step}}(x) = \begin{cases} 0, & 0 \le x < 20\alpha, \\ 1, & 20\alpha \le x \le 20, \end{cases} \qquad p_{\text{Linear}}(x) = 1 - \alpha\left(1 - \tfrac{x}{20}\right),$$
$$p_{\text{Ramp}}(x) = \begin{cases} \frac{x}{20\alpha}, & 0 \le x < 20\alpha, \\ 1, & 20\alpha \le x \le 20. \end{cases} \tag{5}$$

where α is a real parameter between 0 and 1. This parameter does not directly correspond to a singular biological mechanism, it controls how 'extreme' these curves are. Plots of these families of curves are given in Fig. 5a. We will refer to these profiles as 'step', 'linear' and 'ramp', respectively.

For a range of values of α in [0, 1], we analysed 20 simulations for each profile. For values of α close to 0, we expect to see population extinction, as this corresponds to all cells differentiating so the proliferative niche is lost. Additionally, if α is close to 1, the population is likely to proliferate endlessly. So for each profile, there is only a subset of [0, 1] that will give realistic and steady population behaviour. To determine this range for each model, we discarded non-physical results that do not reach steady state within 800 hours (in a 1000 hour simulation) and results that included population extinctions.

Comparisons between each configuration are best represented through plots against the area under the curve of $p(x)$—the total probability of priming across the domain—as this is a useful proxy for the total amount of differentiation that occurs. The results shown in Fig. 5 reveal consistent trends in the population size, composition, and height of the tip-cap unit. For each model, as the area under the curve $p(x)$ increases, the number of total cells decreases, but the number of proliferative cells decreases faster.

From these results, we can see that the mechanics of dynamic equilibrium appear to be the same for a range of parameter values for each type of curve tested. While there is variation in results, the mechanisms of this equilibrium remain schematically indistinguishable. Hence, the choice of curve to use for our model will not influence simulation outcomes, provided $p(x)$ is a non-decreasing function in x. Therefore, we choose to use the simplest function with spatial variance, a step function, for the remainder of this paper.

$$p(x) = \begin{cases} \frac{x}{12}, & 0 \leq x < 12, \\ 1, & 12 \leq x \leq 20. \end{cases} \tag{6}$$

3.3 Adhesion Between CM and UT Cells Results in More Stable Tissues

While interactions between CM and UT cells are known to be important for kidney development, modulating these interactions experimentally is very difficult and has not been addressed. Thus, the importance and specific roles of CM–UT interactions in kidney development is poorly understood. In particular, adhesion between proliferative CM cells and the UT cells is likely to contribute to maintaining steady population dynamics at the ureteric tip. To this end, we investigate the various impacts that this inter-population interaction has on cap mesenchyme population dynamics.

This CM–UT cell adhesion is implemented in the model as follows. When a proliferative CM cell is located at a distance less than h_a from the surface of the tip, it has probability $p_a \, \Delta t$ on each timestep to adhere to the UT cells on the tip surface. When adhered, the damping constant η is magnified by a factor of 100 and the cell is pulled to the surface. Any cell that is adhered to the tip surface has probability $p_d \, \Delta t$ on each timestep to detach from the surface and resume normal behaviour. All probabilities and adhesion are events that are independent of the cell cycle. A state transition diagram summarising these mechanisms is given in Fig. 6a.

We simulated the model for a range of probabilities of attachment and detachment ($0 \leq p_a, p_d \leq 1$) for timestep $\Delta t = 0.005$ and ran 20 simulations for each configuration over 500 hours, results are presented in Fig. 6b–d. It is clear from these results that the dynamics of the system change according to the level of adhesion ($f = p_a/p_d$). Note that $p_a = 0$ disables CM–UT adhesion in the simulation. We also note that simulations with excessive levels of adhesion ($f > 4$) have been discarded, since they produced results with unrealistically high population densities on the tip surface.

As the level of adhesion f increases from 0 to 2, we observe the total population in steady state increases to a local maximum at $f = 0.5$ before decreasing to a local minimum at $f = 2$, which then increases sharply where simulations become unrealistic past $f = 4$. We also observe that the cap height decreases as the level of adhesion f increases across this range of values. Lower levels of adhesion f correspond to simulations where CM cells are less likely to adhere to the surface of the tip and adhere for short periods of time. The increase in total number in steady state is due to the small vertical flows of adhering CM cells, displacing neighbouring cells and thus making room for more successful division events. When the adhesion level f takes values above 1, detachment is less likely than attachment and thus adhered cells stay attached to the UT cells for longer periods of time. Changing the distance of adhesion

h_a (within 20%) did not change the overall behaviour of the system, (results not shown for brevity).

Our investigation of this mechanism in a simplified state shows that adhesion between CM and UT cells temporarily removes dividing cells from the population, controlling the entry rate of cells into the system. These results coincide with biological studies that identify a genetic switch (*Wnt11*) for this adhesion mechanism perturbs CM cells in a similar fashion (O'Brien et al. 2018). Moreover, it pulls the whole population closer to the ureteric tip and increases the density of CM cells around the ureteric tip. That is, increasing CM–UT adhesion interactions leads to less diffusion of the CM cell population from the tip structure, and thus increasing the likelihood of successful niche formation.

4 Discussion

In this section, we reflect on our results in detail and the biological implications and conclusions we can draw from them. In this model of primary cell interactions in the tip-cap unit, we examine the effect of perturbing the magnitude of specific mechanisms and interactions on population totals, composition, and motility, as well as the entry and exit rates of CM cells from the tip-cap unit. In general, a more motile CM population is less likely to lead to the formation of a successful niche, since this relies on specific spatial cues from UT cells. Consistent with this observation, the number of CM cell layers decreases across developmental time (Combes et al. 2016), which is likely to be linked to reduced CM motility. In our model, spatial dependence is sufficient to sustain robust development, and attraction between the cap mesenchyme and the ureteric tip leads to more stable tissues.

4.1 Summary of Simulation Results

Our first point of investigation was the spatial dependence of CM cell differentiation. Division of proliferative CM cells in our model results in two new primed cells with probability p or two proliferative cells with probability $1 - p$. We have shown in Fig. 4 that assuming a spatially independent differentiation probability p and hence implementing uniformly random differentiation of CM cells results in niches that either grow endlessly or approach extinction. Biological niches do not exhibit this behaviour, so additional structure is necessary. We showed that replacing the static differentiation probability p with a simple step function $p(x)$ was sufficient to reproduce realistic niche behaviour, where each simulation attained dynamic equilibrium at similar times and at similar values. Additional parameters in this model can be used to modify the niche size, population size, and composition, thereby giving a general model of niche formation across any stage of ureteric tree development. Some degree of spatial control on differentiation is supported by biological findings (Combes et al. 2016). To further investigate the nature of this spatial dependence on CM differentiation, we examined various parameterised forms of $p(x)$: a step function, a linear function, and a combination of these two. Results obtained and presented in Fig. 5 across values of

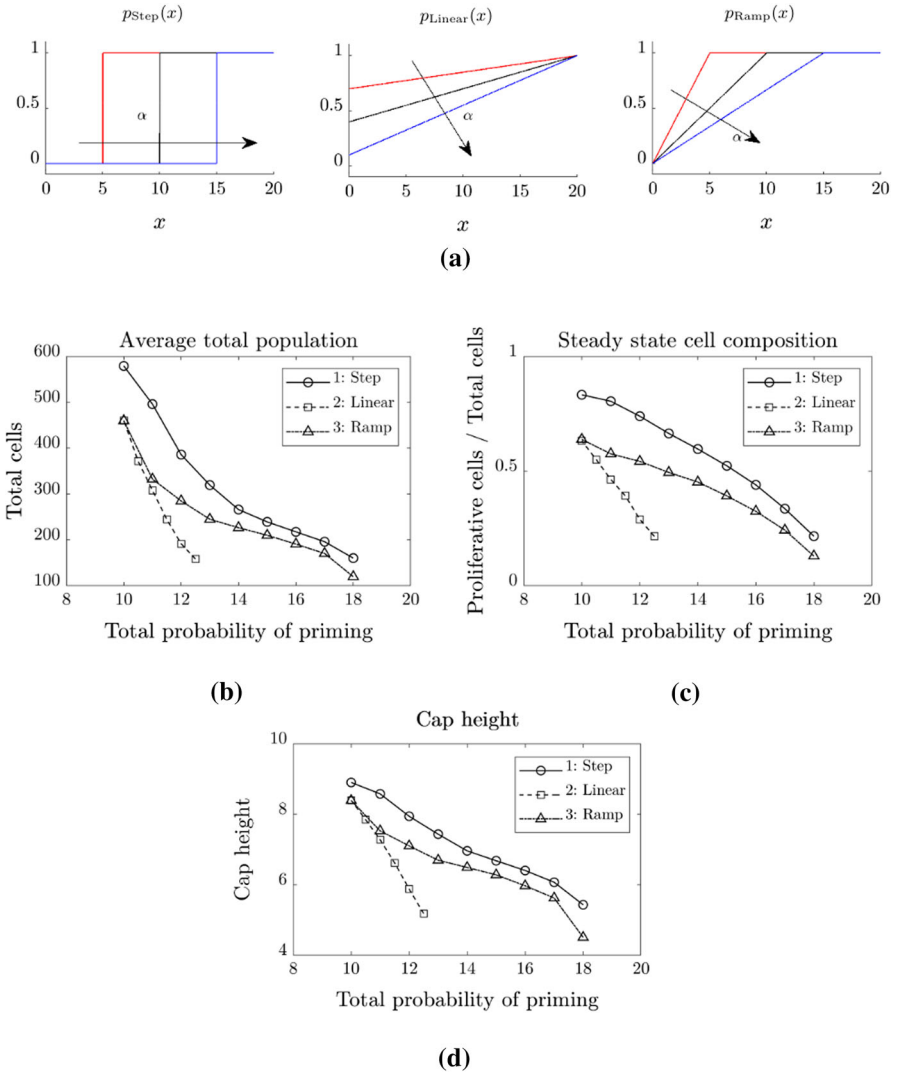

Fig. 5 Plots of the different differentiation response profiles and results as functions of area underneath the response curve. **a** Plots of the step profile, the linear profile, and the ramp profile against x for different values of α, with arrows indicating how the curve changes for increasing values of α. For each profile, the area under the response curve serves as a proxy for α, and represents the total probability of CM cell priming across the simulation domain. Results shown are the total number of cells in steady state (**b**), proliferative proportion of cells (**c**), and the cap height in steady state (**d**). Each response curve produces the same trend as a function of area underneath the curve without overlapping, showing the steady state behaviour is consistent for each non-decreasing response curves tested (Color figure online)

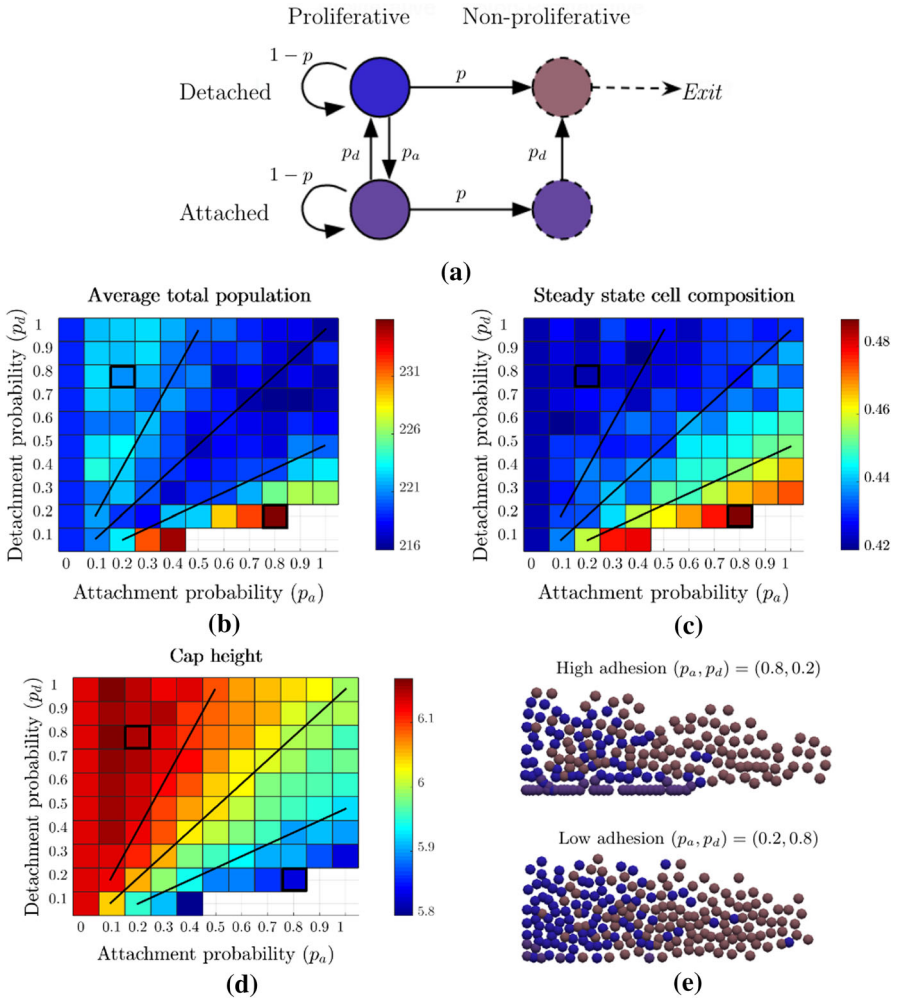

Fig. 6 Adhesion between CM and UT Cells increases tissue stability. **a** State transition diagram of proliferative CM cells on each timestep. **b** average total number of cells in steady state, **c** proportion of proliferative cells in steady state, and **d** average cap height in steady state. The behaviour of the system is dictated by the level of adhesion, given by $f = p_a/p_d$. Black lines overlaid on each plot correspond to simulations with low adhesion ($f = 0.5$), neutral adhesion ($f = 1$) and high adhesion ($f = 2$) from top left to bottom right. Only realistic results are considered here. **e** Snapshots of representative simulations at $t = 500$ at the highlighted regions $(p_a, p_d) = (0.2, 0.8)$ and $(p_a, p_d) = (0.8, 0.2)$ (Color figure online)

area underneath $p(x)$ revealed that each form of non-decreasing $p(x)$ was enough to attain consistent realistic tip-cap behaviour.

In order to investigate the influence of CM–UT adhesion on CM cell population dynamics we implemented a simple stochastic adhesion force between CM cells and the bottom boundary of our model, representing UT cells. We found that our results were dependent on the level of adhesion, given by the ratio $f = p_a/p_d$. When we implement low adhesion ($0 < f < 1$), the population composition and the exit rate of

cells are similar to simulations with no adhesion ($f = 0$). However, the total number of cells and the cap height increase before decreasing as the level of adhesion increases from $f = 0$ to $f = 1$. Simulations configured with high levels of adhesion ($1 < f < 2$) tend to exhibit lower total population numbers, higher numbers of proliferative CM cells, and lower cap heights. We see the simple adhesion mechanics help to stabilise the tip-cap populations. This is due to retention of proliferative/unprimed CM cells on the left of the simulation domain, decreasing the entry rate by maintaining a healthy rate of proliferation and differentiation which in turn help to drive the passive flow of primed cells to the right, increasing the exit rate. Increasing adhesion further ($2 < f < 4$) results in increased total population size and the number of proliferate CM cells, and a continuing decrease in the cap height. Simulations with excessive adhesion ($f > 4$) produced unrealistic results where the underlying assumptions of the model begin to break down due to cells overlapping. Hence, we discarded results in this range.

4.2 Biological Implications

Preliminary investigations of this simplified model of the ureteric tip provide an interesting interpretation from a biological standpoint. Our analysis revealed that additional constraints for differentiation are needed on top of an overcrowding condition. Specifically, a degree of spatial dependence on differentiation was required. This finding has been verified experimentally (Lefevre et al. 2013), showing that this relatively simple cell-based model can replicate the primary dynamics for this complex biological process. Furthermore, the changes in niche size and composition throughout ureteric tree development can be explained by a progressive variation in additional model parameters listed in Table 1.

In addition to this, after implementing a simple adhesion mechanism, our results revealed a significant impact on the composition of the steady state. Increasing the degree of adhesion appeared to have a stabilising effect by retaining unprimed CM cells and thus decreasing the entry rate of new cells. This maintenance of proliferation and differentiation helped drive passive flows of primed CM cells out of the ureteric tip domain, thereby increasing the exit rate. This supports the findings by Combes et al. (2016) and further emphasises the necessity of adhesive properties between CM and UT cells.

4.3 Future Work

Avenues for further development can relax several of the main assumptions used during the construction of this model. For example, the static simulation domain can be revisited and modified to study how the mean behaviour of the cap mesenchyme cells changes across tip development and tip branching. This would better represent the ureteric tip as a dynamic, branching population, and may offer complementary statistical insights alongside the model by Zubkov et al. (2015).

Additionally, we may also wish to revisit the assumptions made on cell migration and plasticity of cell fates. Primed cells have been observed to migrate back to the ‘viable’ central tip region occasionally (Combes et al. 2016), and appear to be able to

return to an unprimed state (Lawlor et al. 2019). One way to investigate this would be to allow primed cells to change back to proliferative cells based on spatial or external cues. As live imaging and cell tracking approaches improve it is likely that a better understanding of how cell migration and cellular interactions change over time, which will enable more accurate comprehensive modelling.

Another avenue of development would be to develop continuum approximations of, or alternatives to, the cell-based system. While such systems would be unable to exhibit the variability seen in our model it would be able to reproduce the mean behaviour and would enable wider investigations to functional forms for $p(x)$ to be undertaken.

5 Conclusions

We have presented a 2-dimensional model of the interactions between cap mesenchyme cells at the interface of the tip of the branches of the ureteric tree in the developing mouse kidney. We have shown that adhesion between cap mesenchyme cells and epithelial ureteric tip cells results in a self-organising structure with a distribution of cells that more closely resembles the physical data than without CM–UT interactions. Our findings line up with established experimental results in this field, suggesting that this simple and general model may lead to more conclusions about cellular interactions on the scale of one tip-cap unit or across the whole ureteric tree.

To conclude, our results provide insight on primary interactions required for maintaining tip-cap dynamics observed in the developing kidney. Moreover, the model constructed provides a base for further multicellular modelling. Further studies can give additional insights on the cellular dynamics of kidney development and how these processes may be manipulated to increase nephron number in at-risk individuals, or to improve tissue engineering in stem cell models of the human kidney.

References

Athreya K, Lahiri S (2006) Measure theory and probability theory. Springer. https://doi.org/10.1007/978-0-387-35434-7

Atwell K, Qin Z, Gavaghan D, Kugler H, Hubbard EJA, Osborne JM (2015) Mechano-logical model of C. elegans germ line suggests feedback on the cell cycle. Development 142(22):3902–3911. https://doi.org/10.1242/dev.126359

Boyle S, Misfeldt A, Chandler KJ, Deal KK, Southard-Smith EM, Mortlock DP, Baldwin HS, de Caestecker M (2008) Fate mapping using Cited1-CreERT2mice demonstrates that the cap mesenchyme contains self-renewing progenitor cells and gives rise exclusively to nephronic epithelia. Developmental Biology 313(1):234–245. https://doi.org/10.1016/j.ydbio.2007.10.014

Cockwell P, Fisher LA (2020) The global burden of chronic kidney disease. The Lancet 395(10225):662–664. https://doi.org/10.1016/S0140-6736(19)32977-0

Combes AN, Davies JA, Little MH (2015) Chapter fourteen cell–cell interactions driving kidney morphogenesis. In: Yap AS (ed) Current topics in developmental biology, cellular adhesion in development and disease, vol 112. Academic Press, pp 467–508. https://doi.org/10.1016/bs.ctdb.2014.12.002

Combes AN, Lefevre JG, Wilson S, Hamilton NA, Little MH (2016) Cap mesenchyme cell swarming during kidney development is influenced by attraction, repulsion, and adhesion to the ureteric tip. Dev Biol 418(2):297–306. https://doi.org/10.1016/j.ydbio.2016.06.028

Cooper FR, Baker RE, Bernabeu MO, Bordas R, Bowler L, Bueno-Orovio A, Byrne HM, Carapella V, Cardone-Noott L, Cooper J, Dutta S, Evans BD, Fletcher AG, Grogan JA, Guo W, Harvey DG, Hendrix M, Kay D, Kursawe J, Maini PK, McMillan B, Mirams GR, Osborne JM, Pathmanathan P, Pitt-Francis JM, Robinson M, Rodriguez B, Spiteri RJ, Gavaghan DJ (2020) Chaste: cancer, heart and soft tissue environment. J Open Source Softw 5(47):1848. https://doi.org/10.21105/joss.01848

Dressler GR (2006) The cellular basis of kidney development. Annu Rev Cell Dev Biol 22(1):509–529. https://doi.org/10.1146/annurev.cellbio.22.010305.104340

Foley RN, Parfrey PS, Sarnak MJ (1998) Clinical epidemiology of cardiovascular disease in chronic renal disease. Am J Kidney Dis 32(5):S112–S119

Hannezo E, Scheele CLGJ, Moad M, Drogo N, Heer R, Sampogna RV, van Rheenen J, Simons BD (2017) A unifying theory of branching morphogenesis. Cell 171(1):242-255.e27. https://doi.org/10.1016/j.cell.2017.08.026

Hildebrandt F (2010) Genetic kidney diseases. The Lancet 375(9722):1287–1295

Jha V, Garcia-Garcia G, Iseki K, Li Z, Naicker S, Plattner B, Saran R, Wang AYM, Yang CW (2013) Chronic kidney disease: global dimension and perspectives. The Lancet 382(9888):260–272. https://doi.org/10.1016/S0140-6736(13)60687-X

Keith DS, Nichols GA, Gullion CM, Brown JB, Smith DH (2004) Longitudinal follow-up and outcomes among a population with chronic kidney disease in a large managed care organization. Arch Intern Med 164(6):659–663

Kobayashi A, Valerius MT, Mugford JW, Carroll TJ, Self M, Oliver G, McMahon AP (2008) Six2 defines and regulates a multipotent self-renewing nephron progenitor population throughout mammalian kidney development. Cell Stem Cell 3(2):169–181. https://doi.org/10.1016/j.stem.2008.05.020

Lam AQ, Freedman BS, Morizane R, Lerou PH, Valerius MT, Bonventre JV (2014) Rapid and efficient differentiation of human pluripotent stem cells into intermediate mesoderm that forms tubules expressing kidney proximal tubular markers. J Am Soc Nephrol 25(6):1211–1225. https://doi.org/10.1681/ASN.2013080831

Lambert B, MacLean AL, Fletcher AG, Combes AN, Little MH, Byrne HM (2018) Bayesian inference of agent-based models: a tool for studying kidney branching morphogenesis. J Math Biol 76(7):1673–1697. https://doi.org/10.1007/s00285-018-1208-z

Lawlor KT, Zappia L, Lefevre J, Park JS, Hamilton NA, Oshlack A, Little MH, Combes AN (2019) Nephron progenitor commitment is a stochastic process influenced by cell migration. Elife 8(e41):156

Lefevre J, Marshall DJ, Combes AN, Ju AL, Little MH, Hamilton NA (2013) Modelling cell turnover in a complex tissue during development. J Theor Biol 338:66–79. https://doi.org/10.1016/j.jtbi.2013.08.033

Lefevre JG, Chiu HS, Combes AN, Vanslambrouck JM, Ju A, Hamilton NA, Little MH (2017) Self-organisation after embryonic kidney dissociation is driven via selective adhesion of ureteric epithelial cells. Development 144(6):1087–1096. https://doi.org/10.1242/dev.140228

Little MH, Combes AN (2019) Kidney organoids: accurate models or fortunate accidents. Genes Dev 33(19–20):1319–1345. https://doi.org/10.1101/gad.329573.119

Mae SI, Shono A, Shiota F, Yasuno T, Kajiwara M, Gotoda-Nishimura N, Arai S, Sato-Otubo A, Toyoda T, Takahashi K, Nakayama N, Cowan CA, Aoi T, Ogawa S, McMahon AP, Yamanaka S, Osafune K (2013) Monitoring and robust induction of nephrogenic intermediate mesoderm from human pluripotent stem cells. Nat Commun 4(1):1367. https://doi.org/10.1038/ncomms2378

Menshykau D, Iber D (2013) Kidney branching morphogenesis under the control of a ligand-receptor-based Turing mechanism. Phys Biol 10(4):46003. https://doi.org/10.1088/1478-3975/10/4/046003

Menshykau D, Michos O, Lang C, Conrad L, McMahon AP, Iber D (2019) Image-based modeling of kidney branching morphogenesis reveals GDNF-RET based Turing-type mechanism and pattern-modulating WNT11 feedback. Nat Commun 10(1):239. https://doi.org/10.1038/s41467-018-08212-8

Mirams GR, Arthurs CJ, Bernabeu MO, Bordas R, Cooper J, Corrias A, Davit Y, Dunn SJ, Fletcher AG, Harvey DG (2013) Chaste: an open source C++ library for computational physiology and biology. PLoS Comput Biol 9(3):100297e0

Müller U, Wang D, Denda S, Meneses JJ, Pedersen RA, Reichardt LF (1997) Integrin $A8\beta1$ is critically important for epithelial-mesenchymal interactions during kidney morphogenesis. Cell 88(5):603–613. https://doi.org/10.1016/S0092-8674(00)81903-0

O'Brien LL, Combes AN, Short KM, Lindström NO, Whitney PH, Cullen-McEwen LA, Ju A, Abdelhalim A, Michos O, Bertram JF, Smyth IM, Little MH, McMahon AP (2018) Wnt11 directs nephron progen-

itor polarity and motile behavior ultimately determining nephron endowment. eLife 7:e40392. https://doi.org/10.7554/eLife.40392

Okuda S, Miura T, Inoue Y, Adachi T, Eiraku M (2018) Combining Turing and 3D vertex models reproduces autonomous multicellular morphogenesis with undulation, tubulation, and branching. Sci Rep 8(1):2386. https://doi.org/10.1038/s41598-018-20678-6

Osborne JM, Fletcher AG, Pitt-Francis JM, Maini PK, Gavaghan DJ (2017) Comparing individual-based approaches to modelling the self-organization of multicellular tissues. PLoS Comput Biol 13(2):1–34. https://doi.org/10.1371/journal.pcbi.1005387

Pathmanathan P, Cooper J, Fletcher A, Mirams G, Murray P, Osborne J, Pitt-Francis J, Walter A, Chapman SJ (2009) A computational study of discrete mechanical tissue models. Phys Biol 6(3):036001. https://doi.org/10.1088/1478-3975/6/3/036001

Purcell EM (1977) Life at low reynolds number. Am J Phys 45(1):3–11

Riccio P, Cebrian C, Zong H, Hippenmeyer S, Costantini F (2016) Ret and Etv4 promote directed movements of progenitor cells during renal branching morphogenesis. PLOS Biol 14(2):e1002382. https://doi.org/10.1371/journal.pbio.1002382

Short KM, Smyth IM (2016) The contribution of branching morphogenesis to kidney development and disease. Nat Rev Nephrol 12(12):754–767. https://doi.org/10.1038/nrneph.2016.157

Short KM, Smyth IM (2017) Imaging, analysing and interpreting branching morphogenesis in the developing kidney. In: Miller RK (ed) Kidney development and disease, results and problems in cell differentiation. Springer, Cham, pp 233–256. https://doi.org/10.1007/978-3-319-51436-9_9

Short KM, Smyth IM (2020) Branching morphogenesis as a driver of renal development. Anat Rec. https://doi.org/10.1002/ar.24486

Short KM, Combes AN, Lefevre J, Ju AL, Georgas KM, Lamberton T, Cairncross O, Rumballe BA, McMahon AP, Hamilton NA, Others Smyth IM, Little MH (2014) Global quantification of tissue dynamics in the developing mouse kidney. Dev Cell 29(2):188–202. https://doi.org/10.1016/j.devcel.2014.02.017

Taguchi A, Kaku Y, Ohmori T, Sharmin S, Ogawa M, Sasaki H, Nishinakamura R (2014) Redefining the in vivo origin of metanephric nephron progenitors enables generation of complex kidney structures from pluripotent stem cells. Cell Stem Cell 14(1):53–67. https://doi.org/10.1016/j.stem.2013.11.010

Takasato M, Er PX, Chiu HS, Maier B, Baillie GJ, Ferguson C, Parton RG, Wolvetang EJ, Roost MS, de Sousa Chuva, Lopes SM, Little MH (2015) Kidney organoids from human iPS cells contain multiple lineages and model human nephrogenesis. Nature 526(7574):564–568. https://doi.org/10.1038/nature15695

Uchiyama Y, Sakaguchi M, Terabayashi T, Inenaga T, Inoue S, Kobayashi C, Oshima N, Kiyonari H, Nakagata N, Sato Y, Sekiguchi K, Miki H, Araki E, Fujimura S, Tanaka SS, Nishinakamura R (2010) Kif26b, a kinesin family gene, regulates adhesion of the embryonic kidney mesenchyme. Proc Natl Acad Sci 107(20):9240–9245. https://doi.org/10.1073/pnas.0913748107

Watson HW, Galton F (1875) On the probability of the extinction of families. J Anthropol Inst Great Britain Ireland 4:138–144

Zandi-Nejad K, Luyckx VA, Brenner BM (2006) Adult hypertension and kidney disease: the role of fetal programming. Hypertension 47(3 II):502–508. https://doi.org/10.1161/01.HYP.0000198544.09909.1a

Zubkov VS, Combes AN, Short KM, Lefevre J, Hamilton NA, Smyth IM, Little MH, Byrne HM (2015) A spatially-averaged mathematical model of kidney branching morphogenesis. J Theor Biol 379:24–37